ChemPubSoc Europe

DOI: 10.1002/cssc.201500155

CHEMSUSCHEM Full Papers

Highly Stable $Na_{2/3}(Mn_{0.54}Ni_{0.13}Co_{0.13})O_2$ Cathode Modified by Atomic Layer Deposition for Sodium-Ion Batteries

Karthikeyan Kaliyappan, Jian Liu, Andrew Lushington, Ruying Li, and Xueliang Sun*[a]

For the first time, atomic layer deposition (ALD) of Al_2O_3 was adopted to enhance the cyclic stability of layered P2-type $Na_{2/3}(Mn_{0.54}Ni_{0.13}Co_{0.13})O_2$ (MNC) cathodes for use in sodium-ion batteries (SIBs). Discharge capacities of approximately 120, 123, 113, and 105 mA h g^{-1} were obtained for the pristine electrode and electrodes coated with 2, 5, and 10 ALD cycles, respectively. All electrodes were cycled at the 1C discharge current rate for voltages between 2 and 4.5 V in 1 M $NaClO_4$ electrolyte. Among the electrodes tested, the Al_2O_3 coating from 2 ALD cycles (MNC-2) exhibited the best electrochemical stability and rate capability, whereas the electrode coated by 10 ALD cycles (MNC-10) displayed the highest columbic efficiency (CE), which exceeded 97% after 100 cycles. The enhanced electrochemical stability observed for ALD-coated electrodes could be a result of the protection effects and high band-gap energy (E_g = 9.00 eV) of the Al_2O_3 coating layer. Additionally, the metal-oxide coating provides structural stability against mechanical stresses occurring during the cycling process. The capacity, cyclic stability, and rate performance achieved for the MNC electrode coated with 2 ALD cycles of Al_2O_3 reveal the best results for SIBs. This study provides a promising route toward increasing the stability and CE of electrode materials for SIB application.

Introduction

As a result of the increasing awareness on global warming and the depletion of fossil fuels, there is much effort devoted to finding alternative energy sources for automobile applications including electric vehicles and hybrid electric vehicles. Rechargeable lithium-ion batteries (LIBs) are considered as an ideal choice for automotive applications, among other battery systems, because of their large capacity and high energy density. However, the high cost and scarcity of lithium reserves has resulted in the pursuit of alternative energy-storage materials.[1] Recently, sodium-ion batteries (SIBs) are drawing attention for use in large-scale energy-storage applications as a result of the abundance and ecofriendly nature of sodium. Furthermore, the intercalation/deintercalation (I/DI) mechanisms of LIBs and SIBs are similar. Henceforth, similar synthetic strategies, materials development, and alloying/conversion chemistry to those utilized for LIBs could also be applied for the development of electrode materials for SIBs.[2] However, SIBs have a number of disadvantages including the larger ionic radius of sodium (≈1.03 Å) and higher redox potential (−2.71 V vs. SHE) relative to the ion size of Li (≈0.79 Å) and redox potential of Li/Li^+ (−3 V vs. SHE).

However, the different interaction mechanism between the host material and Na ions influences the kinetics/thermodynamic properties of SIBs, which provides a new platform for advanced technology to surpass LIBs in high-power applications. The I/DI mechanisms of SIBs and LIBs are almost same, so well-developed lithium-based technology could also be used to explore sodium-based hosts used in SIBs.

Research concerning Na-ion storage into host materials can be traced back to the early 1980s.[3,4] Since that time, a great deal of effort has been devoted to discovering novel sodium-intercalation materials for use in SIBs. Sodium-intercalating host materials, such as layered oxides, transition-metal fluorides, olivine phosphates, pyrophosphate, fluorophosphates, sodium superionic conductors, and alluaudite framework compounds, have been reported as potential cathode materials for SIBs.[3–9] Among the aforementioned materials, layered metal oxides have a number of advantages including facile synthesis, high theoretical capacity, and high working voltage.[5,10–12] Therefore, the exploration of mixed layered oxides as energy-storage materials will advance the construction of high-performance SIBs.

According to Delmas et al., Na-based layered oxide materials can be classified as O3-type and P2-type, in which the Na ions occupy octahedral or prismatic sites, respectively.[13] It was reported that P2-type layered materials exhibit enhanced electrochemical Na-ion storage capability relative to O3-type materials because of the high Na-ion diffusion coefficient and forbidden slab gliding.[14,15] The transition-metal intermixing component, for example, in $NaNi_{1/3}Mn_{1/3}Fe_{1/3}O_2$, displays a number of favorable features such as stable structure and higher capacity than in the Li counterpart.[7] This may be a result of the combination of the several advantages from the different metals and the elimination of the drawbacks and challenges related to the pure oxides.[2,3] Hence, focus has been made to develop these

[a] Dr. K. Kaliyappan, Dr. J. Liu, A. Lushington, R. Li, Prof. X. Sun
Department of Mechanical and Materials Engineering
University of Western Ontario
London, Ontario, N6A 5B9 (Canada)
E-mail: xsun@eng.uwo.ca

Supporting Information for this article is available on the WWW under http://dx.doi.org/10.1002/cssc.201500155.

intermixing layered metal-oxide cathode materials.[7] Recently, numerous sodium-intercalation P2-type materials, such as $NaMO_2$ (M: Cr, Fe, Co, and Ni), $Na_{0.67}(Mn_{0.65}Co_{0.2}Ni_{0.15})O_2$, $Na_{2/3}(Mn_{1/2}Fe_{1/2})O_2$, $Na_{2/3}(Ni_{1/3}Mn_{2/3})O_2$, $Na_{2/3}Ni_{1/3}Mn_{2/3-x}Ti_xO_2$, and $Na_{0.67}Mn_{0.65}Fe_{0.2}Ni_{0.15}O_2$ have been demonstrated to store Na ions in their structure.[2,3,9,14,16–18] Despite delivering high capacity, these materials experience severe capacity decay even at a low current density and simultaneously demonstrate poor rate performance. Furthermore, the limitations of these materials at high cutoff voltages hinder their application in the fabrication of high-energy-density SIBs.

Many strategies have been applied to address the above challenges. Wang et al. proposed that the severe capacity fading observed under elevated voltage conditions is a result of crystal structure changes that occur during the charge/discharge (C–DC) process.[19] They also noted that the unstable electrochemical behavior of layered electrode materials cycled at voltages of between 2 and 4.5 V results in an irreversible phase transformation at voltages greater than 4.3 V. Lu and Dhan also suggested that capacity retention is greatly affected by the P2–O2 phase transformation at voltages above 4.2 V.[20] To stabilize the structure, small-sized cations implemented into the host structure have been shown to be successful. Yuan et al. and Yoshida et al. demonstrated that doping Al and Ti into P2-type $Na_{0.67}[Mn_{0.65}Co_{0.2}Ni_{0.15}]O_2$ and $Na_{2/3}Ni_{1/3}Mn_{2/3-x}Ti_xO_2$, respectively, stabilized the structures for high-voltage operation at 4.2 V.[17,18] Although cation doping enhances structural stability, the rate capability of these material is still not adequate for practical applications because of the large particle size, uneven particle shape and distribution, and severe particle agglomeration.[17,18]

Previous reports have indicated that the preparation method and surface morphology have a large influence on the electrochemical performance of any cathode materials.[21] The preparation of cathode materials with uniform structure and high crystallinity is an ideal path to enhancing the C–DC performance of intercalation host materials.[22] By following this methodology, we have succeeded in synthesizing micrometer-sized P2-type $Na_{2/3}(Mn_{0.54}Ni_{0.13}Co_{0.13})O_2$ (MNC) with uniform size and distribution with a citric acid assisted sol–gel method. The citric acid acted as a chelating agent to reduce the particle agglomeration and to upsurge the structural integrity of the final product. Unfortunately, the MNC cell experienced capacity fading during the cycling process at voltages above 4.3 V. One effective way to improve the electrochemical stability of SIB cathodes is to introduce a surface coating layer. This additional layer protects the active electrode material from hazardous reaction byproducts that are produced during the C–DC process.[23] Numerous reports have indicated that the use of conductive carbon and/or metal oxides on the surface as a coating results in enhanced cycling stability for various energy-storage materials.[24,25] However, the presence of inactive carbon on the surface decreased the initial capacity value.[26] On the other hand, metal-oxide coatings not only improve the electrochemical stability of the cathode but also increase the initial capacity value.[27] Moreover, these rigid coatings can aid in maintaining the mechanical integrity of the cathode during the C–DC process. Traditionally, solution-based coating methods, such as sol–gel and hydrothermal methods, are adopted to deposit metal-oxide coatings on the surface of cathode materials.[23,28] However, uniform coatings are difficult to produce by using conventional coating methods, which result in rough surface coatings that inadequately protect the surface. In addition, these solution-based methods require a large amount of precursor and solvent, as well as subsequent heat treatment.[23,28]

Atomic layer deposition (ALD) is a technique that has recently been used to coat metal oxides on anode and cathode materials for LIB applications. ALD has the excellent capability of coating thin films at the atomic scale along with unprecedented uniformity.[29] Additionally, metal-oxide coatings by ALD have led to enhanced electrochemical lithium-ion-storage capability for various anode and cathode materials for LIBs.[29,30] Various metal-oxide coatings (Al_2O_3, ZrO_2, TiO_2, and $LiTaO_3$) have been applied by using the ALD method on different anodes and cathodes for high-performance LIB applications.[31–34] Although the ALD method has been employed in various energy-storage applications, such as LIBs, fuel cells, and lithium–sulfur batteries, coating of metal oxides on SIB cathodes with ALD has not yet been explored.[33,35–38] Han et al. reported the ALD of an Al_2O_3 thin film on an Sn nanostructured anode for SIBs, along with improved cycling performance.[39] However, the use of ALD metal-oxide coatings for SIB cathodes has not yet been reported. In addition, the adoption of the ALD technique will open wide channels for developing high-energy-density materials with enhanced stability for SIBs, because the capacity retention normally decreases with the upper voltage limit.

In this regard, we are reporting ALD coating of alumina (Al_2O_3) on MNC electrodes as high-performance cathode materials for SIBs. To the best of our knowledge, this is the first report of ALD-controlled metal-oxide coating on sodium-based P2-type layered oxide intercalation electrodes. In particular, emphasis is placed on studying the effect of the ALD coating thickness on the electrochemical characteristics for SIBs. It was reported that direct ALD on as-prepared powders results in slower ionic and electronic transport as a result of the inherent properties of the metal oxide preventing a continuous network from being formed.[40,41] Based on this, we have coated Al_2O_3 thin films with different thicknesses directly on the MNC electrode by using ALD. This work evaluated the effect of ALD coating thickness on the cycling performance and rate capability of MNC materials versus a metal Na anode in 1 M $NaClO_4$ electrolyte. Additionally, capacity fading is more obvious at high voltage cycling because of the harmful reactions with the electrolyte and dissolution of active species into the electrolyte. High-potential operation is more demanding for large-scale storage applications, so we have chosen 4.5 V as the upper-cutoff voltage limit for the present study. The obtained results revealed that ultrathin Al_2O_3 films can dramatically enhance the electrochemical stability of pristine MNC cathodes at high operating voltages. In addition, the columbic efficiency (CE) of the electrodes increased linearly with number of ALD cycles. The impact of Al_2O_3 film thickness on the electrochemical conductive profile was also determined.

Results and Discussion

Figure 1a displays an SEM image of MNC powder prepared by using the citric acid assisted sol–gel method at $T=850\,^{\circ}C$ for 12 h. Figure 1a confirms that the pristine MNC displays well-defined particles with very smooth surfaces and edges. An average particle size of approximately 1.5 μm was observed from Figure 1a. The image also illustrates that the prepared powder has uniform particle size and distribution, which results from the addition of citric acid during the synthesis process. This type of morphology decreases particle agglomeration and aids in reducing the distance for ionic migration. It has been reported that the ion insertion into the host material is mainly dominated by the ion diffusion distance.[21,22,33,34,37] However, after Al_2O_3 ALD coating, the surface of the MNC particles becomes rough, as shown in Figure 1b and Figure S1 in the Supporting Information. The homogeneity of the MNC powder and the existence of the Al_2O_3 coating layer on the surface was analyzed by energy-dispersive X-ray spectroscopy (EDX). Figure S2 in the Supporting Information shows the EDX mapping of MNC powders synthesized with the sol–gel method at $T=850\,^{\circ}C$ for 12 h and illustrates the Mn-, Co-, Ni-, and Na-ion distributions with similar intensities, which indicates the molecular-level mixing of the starting materials. The presence of Al on the surface of the MNC particles was also confirmed by EDX (Figure S3–S5 in the Supporting Information) and the intensity of Al increases with the number of ALD cycles. A similar trend was also observed in the EDX profile presented in Figure S6 in the Supporting Information. To further confirm the coating layer on the MNC surface, high-resolution TEM (HRTEM) was conducted on the MNC-10 sample and the corresponding image is shown in Figure 1c. The HRTEM image shows the presence of a thick Al_2O_3 coating of approximately 1.5 nm on the MNC-10 surface.[31,33,36,38] In addition, Figure S7 in the Supporting Information clearly reveals that it is hard to observe the Al_2O_3 coating layer for the electrode coated with 2 ALD cycles as a result of the relative thinness of the coating layer.[31,32] We have reported in our previous study that the growth rate of the Al_2O_3 coating per cycle of ALD was approximately 0.13 nm.[33] However, it is apparent for the MNC-5 and MNC-10 samples that the thickness of the coating layer was increased if the number of ALD cycles was increased.

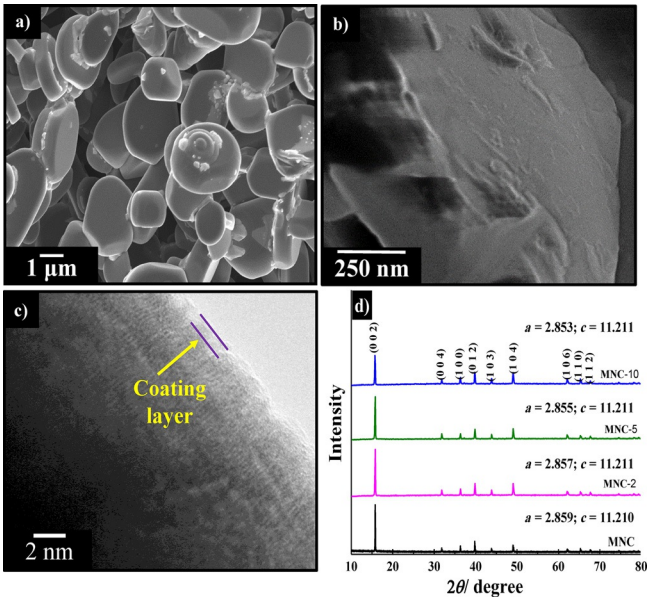

Figure 1. SEM images of a) MNC and b) MNC-10 particles; c) TEM image of MNC-10 particle; d) XRD patterns of pristine MNC and Al_2O_3-coated MNC samples. The lattice parameters are inserted above the spectra.

The XRD patterns of pristine MNC and ALD-coated MNC powders are presented in Figure 1d. As seen from Figure 1d, the pristine MNC displays characteristic peaks for a hexagonal structure with the $P6_3/mmc$ space group (JCPDS PDF no. 194), as reported by several authors.[14,17,18] In addition, sharp and intense peaks confirm the formation of highly crystalline MNC powders. The ALD-coated MNC also displays a hexagonal structural behavior. Furthermore, peaks associated to the Al_2O_3 coating material are not observed in the XRD patterns of MNC-2, MNC-5, and MNC-10 because of the ultrathin and amorphous nature of the Al_2O_3 coating layers.[34] The lattice parameters (*a* and *c*) of the pristine and ALD-coated materials were also calculated from the XRD patterns and are shown in Figure 1d. The lattice parameters of all samples is almost the same, which demonstrates that surface modification of the ALD Al_2O_3 coating at $T=100\,^{\circ}C$ did not affect the structure of the MNC. It is well known that high working voltage and large capacity are necessary to utilize any cathode materials for high-energy applications. Figure S8 in the Supporting Information presents the C–DC curves and cycling performance of the pristine MNC electrode cycled at different voltage ranges of 2–4.3 V and 2–4.5 V at 1C discharge current rate for 100 cycles. The MNC electrode delivered discharge capacities of 81 and 121 $mA\,h\,g^{-1}$ between the voltage ranges of 2–4.3 and 2–4.5 V, respectively. If cycled between 2 and 4.3 V, the cell displayed exceptional cycling stability after 100 cycles, as illustrated in Figure S8b in the Supporting Information. In contrast, the MNC electrode cycled between the 2–4.5 V voltage range experienced severe capacity decay upon cycling, most likely as a result of structural changes and dissolution of active species during the C–DC process.[19,20] Despite monotonous capacity fading in the high voltage window of 2–4.5 V, the capacity and cycling performance achieved at 1C is the best reported value for P2-type layered materials used in SIBs.[19,20] It is apparent that the long-term cyclability is an important parameter for energy-source materials along with a high capacity value. Nevertheless, the poor cycling stability and cutoff voltage limitations of pristine MNC electrode restricted their practical application. Therefore, Al_2O_3 coatings with different thicknesses were adopted to improve the cycling stability of the pristine MNC electrode and the results are discussed in the following section.

The C–DC voltage profiles of pristine and ALD-coated electrodes recorded at 1C and voltages between 2 and 4.5 V in 1 M $NaClO_4$ electrolyte are shown in Figure 2a. All of the cells demonstrate three distinctive slopes and plateaus during the charge process. The presence of high Mn content caused

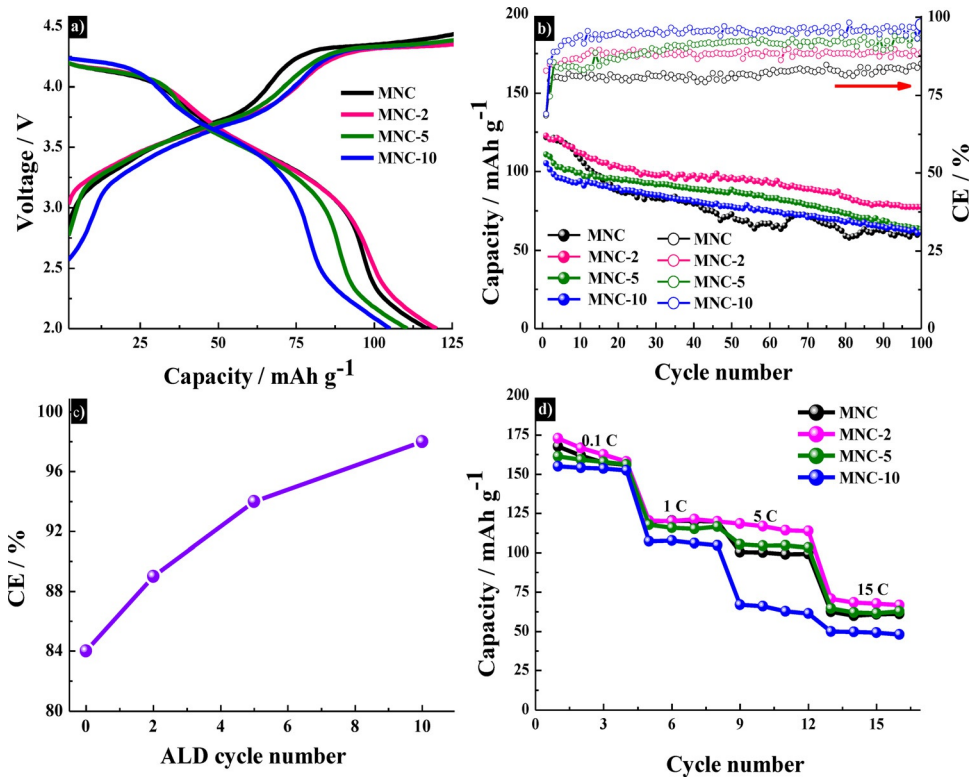

Figure 2. a) Initial C–DC analysis at 1C; b) cyclic performance of the electrodes at 1C for 100 cycles; c) columbic efficiency (CE) of the electrodes with different ALD coating thicknesses; d) rate capabilities of the MNC, MNC-2, MNC-5, and MNC-10 electrodes measured within the potential range of 2–4.5 V at different discharge current rates.

a longer plateau as a result of the Mn^{3+}/Mn^{4+} redox couple. Moreover, redox peaks associated to the Ni^{2+}/Ni^{4+} and Co^{3+}/Co^{4+} couples can be observed at voltages of 4.3 and 3.6 V, respectively. Meanwhile, the discharge plateau also displays a clear downwards slope along with three reduction peaks, which indicates the complex nature of the electrochemical reactions in P2-type layered materials.[14,16–18,41] This complex electrochemical reaction of the layered materials originates from the gliding of oxygen planes and the Na-ion vacancy ordering.[42] There were irreversible capacity losses observed for all cells tested. Generally, the irreversible capacity loss during the initial cycles can be attributed to the possible irreversible reactions such as decomposition of the electrolyte, which results in the formation of a solid electrolyte interphase (SEI).[21,22] As shown in Figure 2a, a discharge capacity of approximately 121 mA h g^{-1} was obtained from the pristine MNC electrode at 1C in the 2–4.5 V potential range, whereas the MNC-2, MNC-5, and MNC-10 electrodes displayed discharge capacities of approximately 123, 110. and 105 mA h g^{-1} under the same testing conditions. The discharge capacity of the ALD-coated electrode linearly decreases with the increasing number of ALD cycles. This trend is associated with the presence of a thick inactive Al_2O_3 film on the surface of the electrode, as seen from the HRTEM images in Figure S7 in the Supporting Information.[30,33,37] In addition, the ultrathin ALD coating of Al_2O_3 (2 cycles of ALD coating) exhibits enhanced electrochemical activity over that of the electrodes with thicker ALD coatings.[34,40] In other words, the thicker Al_2O_3 layers inhibit the diffusion of Na ions into the bulk active material, which leads to reduced availability of the active species to participate in electrochemical charge-storage reactions.[31,34,37,40] Consequently, the capacity was decreased for the MNC electrode coated with 10 ALD cycles.

The impact of ALD coating on the cyclic stability was also examined at 1C for 100 cycles within a potential range of 2–4.5 V. It is evident from Figure 2b that the pristine MNC electrode showed severe capacity fading with only 50% capacity retention after 100 cycles. This continuous capacity decay was caused by the structural changes of MNC during the electrochemical C–DC process.[19,20] As expected, ALD-coated MNC electrodes display higher capacity retention than the pristine MNC electrode. Among the ALD-coated electrodes, the MNC electrode coated with 2 ALD cycles (MNC-2) has better cyclic stability than the pristine MNC electrode at 1C. Interestingly, the MNC-10 electrode showed lower discharge capacity but better cyclability after 100 cycles. The enhanced stability of the MNC-10 sample results from the influence of the thicker ALD coating, which effectively eliminated the phase transformation and thus increased the cyclic stability of the MNC-10 electrode. The CE values of the electrodes after 100 cycles were also improved with an increase in the number of ALD cycles, as presented in Figure 2c.

The pristine MNC electrode has a CE value of approximately 84% after 100 cycles. Conversely, the MNC-2, MNC-5, and MNC-10 electrodes showed CE values of 89, 94, and 98%, respectively, after 100 cycles at 1C. Sun and co-workers reported that the thicker Al_2O_3 coating layer not only protects the electrode from electrolyte attack but also reduces the use of active species, which results in higher CE values.[37] It is clear from the C–DC curves that surface modification with ultrathin Al_2O_3 is advantageous for improving the stability of P2-type layered MNC electrodes, especially at high working voltages. The ultrathin Al_2O_3 layer on the MNC electrode prevented direct contact between MNC particles and the electrolyte solution and, thus, effectively hindered the dissolution of the ion-conductive SEI, minimized the consumption of active materials into the electrolyte, and increased the discharge capacity and cyclic stability of the pristine material. In addition, the electrical band structure of ALD-coated Al_2O_3 also influenced the performance of the MNC electrodes. Al_2O_3 has a higher band-gap energy of

9.00 eV, so phase transformations are suppressed during the C–DC process and, hence, cyclic stability is improved.[33,43] Besides this, the coating layer provided a flexible structure against the mechanical strain and stress formed during the cycling process, which led to better electrochemical behavior.[27,31,33] This enhanced the cyclic performance of the pristine electrode by eliminating the formation of void spaces between the cathode and conductive additives.[33,34,38,44]

Furthermore, the ALD coating effectively prevents the structural transformation upon cycling, which leads to an increase in capacity retention. A similar trend was also observed in the rate performance studies. Figure 2d shows the rate performance of pristine and ALD-coated electrodes under different current densities ranging from 0.1 to 15C. As the discharge current rate increases, the capacity of the cells decreases, which demonstrates that a surface-adsorption phenomena is occurring. This may restrict the full utilization of active materials at high discharge current rates for charge-storage reactions.[33,45] The results obtained from the rate-performance study indicate that the MNC-2 electrode displays higher capacity values than the pristine MNC, MNC-5, and MNC-10 electrodes as a result of an increase in conductivity (Figure 2d). Additionally, electrolyte oxidation at high discharge current rates is severe and results in rapid SEI film erosion. The dissolution of the SEI film leaves the active species able to interact directly with the acidic electrolyte and, thereby, the discharge capacity is enormously reduced upon subsequent cycling progress.[28] A high capacity of approximately 72 mA h g^{-1} was observed for the electrode coated with 2 ALD cycles at 15C. Unfortunately, the MNC-10 electrode delivered the lowest capacity value. This may be a result of the thick insulating Al_2O_3 layer.[30,33,36–40,45] From the C–DC and rate performance analysis, it can be concluded that 2 ALD cycles of Al_2O_3 coating are optimal for obtaining high-rate-performance electrodes for large-scale SIB applications.[34,37,38]

To further analyze the electrochemical nature of pristine and ALD-coated electrodes, CV measurements were conducted at voltages between 2 and 4.5 V at a scan rate of 0.1 mV s^{-1}. The CV curves of all electrodes for the first cycle are illustrated in Figure 3a. The CV traces clearly reveal the complexity of the electrochemical I/DI of the Na ions into the MNC structure. All curves display three primary redox processes and a sharp insertion peak during the reverse scan, which agrees well with the results obtained from the C–DC studies.[42]

The redox peaks centered at voltages of approximately 2.3, 3.6, and 4.3 V can be assigned to the electrochemical redox reactions of $Mn^{3+/4+}$, $Co^{3+/4+}$, and $Ni^{2+/4+}$, respectively.[46] The electrochemical oxidative current response area of samples coated by 2 ALD cycles was higher than that of the pristine MNC-5 and MNC-10 electrodes, which demonstrated the excellent electrochemical activity of MNC-2 and is similar to the additional charging capacity obtained during the C–DC studies. Analogous behavior is observed during the reduction reaction as well. Moreover, the pristine electrode showed peak shifts in both positive and negative scans, which confirms the lower electrochemical polarization of the pristine electrode that leads to unstable Na-ion I/DI behavior. These interpretations agree

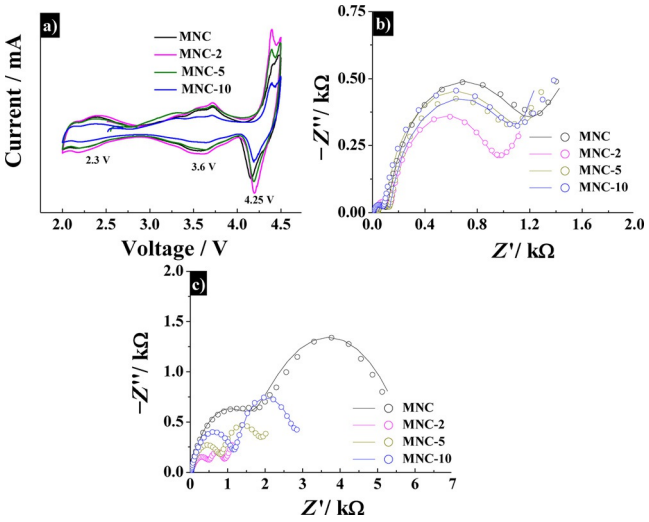

Figure 3. a) CV traces of the cells fabricated with MNC and Al_2O_3-coated MNC electrodes at potential ranges between 2 and 4.5 V at a scan rate of 0.1 mV s^{-1}; Nyquist plots of the MNC, MNC-2, MNC-5, and MNC-10 electrodes recorded b) before and c) after cycling at 1C for 100 cycles, respectively. The scatter and line curves represent experimental and fitted data, respectively.

well with the results obtained during the C–DC process and rate performance studies.

The influence of the Al_2O_3 coating thickness on the conductive profile was examined through electrochemical impedance spectroscopy (EIS) measurement before the C–DC process. Figure 3b shows the Nyquist plots for the pristine MNC and Al_2O_3-coated MNC electrodes conducted at open circuit voltage between a frequency range of 200 kHz to 10 mHz. All of the spectra contain three regions: semicircles in the lower- and medium-frequency regions and a line inclined at approximately 45° to the real axis in the high-frequency region. The lower- and medium-frequency semicircles can be assigned to ionic migration resistance (R_{sf}) through the SEI layer and charge-transfer resistance (R_{ct}) at the cathode–electrolyte interface, respectively. The inclined line at the high-frequency region (Warburg impedance Z_W) is attributed to Na-ion diffusion into the bulk of the electrode material. The EIS curves are fitted according to the equivalent circuit given in Figure S9 in the Supporting Information and the parameters are summarized in Table 1. The parameters R_s, Q_1, and Q_2 are associated to the ohmic resistance, interfacial capacitance, and double-layer capacitance, respectively. Generally, interfacial capacitance refers to the charge transfer through the bulk electrode, whereas the double-layer capacitance is related to the charge transfer between the electrode and electrolyte interface. It was demonstrated that the increase of interfacial resistance was an indication of increased interfacial charge-transfer resistance, which could be used to predict the cycling stability of any electrode materials.[47] As seen in Table 1, the MNC-2 electrode had a low interfacial-resistance value among the electrodes tested, which reveals that interfacial resistance significantly improves after ultrathin Al_2O_3 coating (2 cycles of ALD). The stabilized SEI layer of the pristine MNC electrode thereby enhances the cyclic performance of the cell. The electrochemical parameters in Table 1

Table 1. Electrochemical impedance parameters of the MNC, MNC-2, MNC-5, and MNC-10 electrodes recorded before and after cycling at 1C for 100 cycles.

Electrode	Before cycling				After cycling			
	$Q_1\times10^{-6}$ [$\mu F\,cm^{-2}$]	$Q_2\times10^{-3}$ [$\mu F\,cm^{-2}$]	R_s [Ω]	R_{ct} [Ω]	$Q_1\times10^{-6}$ [$\mu F\,cm^{-2}$]	$Q_2\times10^{-3}$ [$\mu F\,cm^{-2}$]	R_s [Ω]	R_{ct} [Ω]
pristine MNC	37.58	0.696	92.3	1102.5	13.23	0.251	2757.5	3147.9
MNC-2	22.06	0.593	116.5	1069.9	0.82	46.31	644.3	505.5
MNC-5	23.73	0.826	101.8	1354.4	1.02	23.07	1018.4	1459.2
MNC-10	28.51	0.935	114.6	1487.7	1.1	26.26	1472.8	1742.1

show small variations in the R_s value as a result of the complex reaction mechanism of the Na ions in the electrolyte.[21,22] However, a clear difference is noted in the resistance associated to the R_{ct} value, which arises from the effect of surface modification by Al_2O_3 deposition. Table 1 indicates that the R_{ct} values linearly increased with an increase in the coating thickness. Li et al. and Xiao et al. demonstrated by using synchrotron-based X-ray photoelectron spectroscopy that the ultrathin ALD coating (2 ALD cycles) is more favorable for forming an effective protection layer on the surface of electrodes, which also supported an enhancement of the Na-ion diffusion rate and effectively protected the SEI layer.[37,48] In contrast, MNC-10 with a thick insulating coating layer increased the R_{ct} value by decreasing the participation of active material for electrochemical reaction.[48] Hence, improved electrochemical performance was noted from the MNC electrode coated with 2 ALD cycles of Al_2O_3 film.

The EIS analysis was also performed for the electrodes after cycling at 1C within a potential range of 2–4.5 V for 100 cycles and the corresponding Nyquist plots are presented in Figure 3c. The Nyquist plots of the pristine and Al_2O_3-coated electrodes after cycling show a clear difference (Figure 3b and c). In particular, the R_s value displays a large difference, as listed in Table 1. This can be attributed to an increase in resistance as a result of the presence of the insulating coating layer.[44] Moreover, the R_{sf} value is mainly related to the resistance for Na-ion diffusion through the SEI film. It is clear from Figure 3c that the pristine MNC electrode has a larger R_{sf} value than any ALD-coated electrodes, which demonstrates severe damage of the SEI layer during electrochemical cycling. According to Li et al., the large difference in the R_{sf} value for the ALD-coated electrodes is due to the presence of byproduct derived from the decomposition of the coating layer along the electrolyte decomposition products.[33,34,44,49] Furthermore, the R_{sf} value of the electrode is increased an increase in the number of coating layers from 2 to 10 cycles, which confirms the presence of more byproduct formed by Al_2O_3-coating decomposition; this is in good agreement with the above justification and the previous reports.[34,49] In contrast, the MNC-2 electrode exhibited lower R_{ct}, whereas the MNC-10 electrode has a larger R_{ct} value, which demonstrates that the thicker Al_2O_3 coating layer blocked the active reaction sites from participating in the charge-storage reaction.[29,33,34,36–38,44] Therefore, the thin coating layer not only protects the electrode surface from metal dissolution but also stabilizes SEI formation, even after the cycling process. This results in an increase in Na-ion storage relative to that of the pristine MNC electrode.[33,38,45] These results clearly reveal that ALD coating has a significant impact on the cyclic behavior of the pristine electrode, especially in a high cutoff voltage range, and could be used to develop high-energy-density SIBs, which could be utilized for large-scale applications.

Conclusions

A surface-modification strategy has been applied to enhance the cyclic stability of a pristine P2-type $Na_{2/3}(Mn_{0.54}Ni_{0.13}Co_{0.13})O_2$ (MNC) electrode for high-performance sodium-ion batteries (SIBs). A series of atomic layer deposition (ALD) cycles of Al_2O_3 were employed on MNC electrodes and the Na-ion storage capabilities of the ALD-coated electrodes were tested with C–DC studies within a potential range of 2–4.5 V at different discharge current rates. Among the electrodes, the MNC-2 electrode displayed the highest discharge capacity of 123 $mA\,h\,g^{-1}$ at 1C, as well as excellent cyclic stability, which is the best ever reported performance for P2-type electrodes cycled at voltages above 4.2 V. The discharge capacities and rate capabilities decreased if the number of ALD cycles was increased. The decreasing capacity trend resulted from the presence of a thick insulating layer on the surface of the electrode. The thicker ALD Al_2O_3 coating also reduced the utilization of active materials and increased the charge-transfer resistance upon cycling, which correlated well with the results obtained from impedance studies. Based on the present investigation, it can be inferred that the application of ALD coating on cathodes is a promising approach to fabricate high-performance SIBs for future applications.

Acknowledgements

This work was supported by Nature Sciences and Engineering Research Council of Canada (NSERC), Canada Research Chair (CRC) Program, Canada Foundation for Innovation (CFI), Ontario Research Fund (ORF), the Canadian Centre for Electron Microscopy (CCEM) at McMaster University, and the University of Western Ontario.

Keywords: aluminum · atomic layer deposition · batteries · electrochemistry · sodium

[1] M. Armand, J. M. Tarascon, *Nature* **2008**, *451*, 652–657.
[2] S. Y. Hong, Y. Kim, Y. Park, A. Choi, N.-S. Choi, K. T. Lee, *Energy Environ. Sci.* **2013**, *6*, 2067–2081.
[3] S. Miyazaki, S. Kikkawa, M. Koizumi, *Synth. Met.* **1983**, *6*, 211–217.
[4] S. Kikkawa, S. Miyazaki, M. Koizumi, *J. Power Sources* **1985**, *14*, 231–234.
[5] P. Barpanda, G. Liu, C. D. Ling, M. Tamaru, M. Avdeev, S.-C. Chung, Y. Yamada, A. Yamada, *Chem. Mater.* **2013**, *25*, 3480–3487.
[6] V. Palomares, P. Serras, I. Villaluenga, K. B. Hueso, J. Carretero-Gonzalez, T. Rojo, *Energy Environ. Sci.* **2012**, *5*, 5884–5901.

[7] V. Palomares, M. Casas-Cabanas, E. Castillo-Martinez, M. H. Han, T. Rojo, *Energy Environ. Sci.* **2013**, *6*, 2312 – 2337.
[8] S. M. Oh, S. T. Myung, J. Hassoun, B. Scrosati, Y. K. Sun, *Electrochem. Commun.* **2012**, *22*, 149 – 152.
[9] S.-W. Kim, D.-H. Seo, X. Ma, G. Ceder, K. Kang, *Adv. Energy Mater.* **2012**, *2*, 710 – 721.
[10] K. Chihara, A. Kitajou, I. D. Gocheva, S. Okada, J.-i. Yamaki, *J. Power Sources* **2013**, *227*, 80 – 85.
[11] A. Gupta, C. Buddie Mullins, J. B. Goodenough, *J. Power Sources* **2013**, *243*, 817 – 821.
[12] H. Yoshida, N. Yabuuchi, S. Komaba, *Electrochem. Commun.* **2013**, *34*, 60 – 63.
[13] C. Delmas, C. Fouassier, P. Hagenmuller, *Physica B+C* **1980**, *99*, 81 – 85.
[14] N. Yabuuchi, M. Kajiyama, J. Iwatate, H. Nishikawa, S. Hitomi, R. Okuyama, R. Usui, Y. Yamada, S. Komaba, *Nat. Mater.* **2012**, *11*, 512 – 517.
[15] M. Sathiya, K. Hemalatha, K. Ramesha, J. M. Tarascon, A. S. Prakash, *Chem. Mater.* **2012**, *24*, 1846 – 1853.
[16] D. Yuan, X. Hu, J. Qian, F. Pei, F. Wu, R. Mao, X. Ai, H. Yang, Y. Cao, *Electrochim. Acta* **2014**, *116*, 300 – 305.
[17] D. Yuan, W. He, F. Pei, F. Wu, Y. Wu, J. Qian, Y. Cao, X. Ai, H. Yang, *J. Mater. Chem. A* **2013**, *1*, 3895 – 3899.
[18] H. Yoshida, N. Yabuuchi, K. Kubota, I. Ikeuchi, A. Garsuch, M. Schulz-Dobrick, S. Komaba, *Chem. Commun.* **2014**, *50*, 3677 – 3680.
[19] H. Wang, B. Yang, X.-Z. Liao, J. Xu, D. Yang, Y.-S. He, Z.-F. Ma, *Electrochim. Acta* **2013**, *113*, 200 – 204.
[20] Z. Lu, J. R. Dahn, *J. Electrochem. Soc.* **2001**, *148*, A1225 – A1229.
[21] K. Karthikeyan, S. Amaresh, S. H. Kim, V. Aravindan, Y. S. Lee, *Electrochim. Acta* **2013**, *108*, 749 – 756.
[22] K. Karthikeyan, S. Amaresh, G. W. Lee, V. Aravindan, H. Kim, K. S. Kang, W. S. Kim, Y. S. Lee, *Electrochim. Acta* **2012**, *68*, 246 – 253.
[23] J. Cho, Y. J. Kim, B. Park, *Chem. Mater.* **2000**, *12*, 3788 – 3791.
[24] B. L. Ellis, W. R. M. Makahnouk, Y. Makimura, K. Toghill, L. F. Nazar, *Nat. Mater.* **2007**, *6*, 749 – 753.
[25] J.-J. Ding, Y.-N. Zhou, Q. Sun, Z.-W. Fu, *Electrochem. Commun.* **2012**, *22*, 85 – 88.
[26] Y. Lu, S. Zhang, Y. Li, L. Xue, G. Xu, X. Zhang, *J. Power Sources* **2014**, *247*, 770 – 777.
[27] S. Amalraj, R. Sharabi, H. Sclar, D. Aurbach in *Electrolytes for Lithium and Lithium-Ion Batteries* (Eds.: T. R. Jow, K. Xu, O. Borodin, M. Ue), Springer, New York, **2014**, pp. 283 – 321.
[28] S. Amaresh, K. Karthikeyan, K. J. Kim, K. S. Nahm, Y. S. Lee, *RSC Adv.* **2014**, *4*, 23107 – 23115.
[29] X. Meng, X.-Q. Yang, X. Sun, *Adv. Mater.* **2012**, *24*, 3589 – 3615.
[30] Y. S. Jung, A. S. Cavanagh, A. C. Dillon, M. D. Groner, S. M. George, S.-H. Lee, *J. Electrochem. Soc.* **2010**, *157*, A75 – A81.
[31] D. Wang, J. Yang, J. Liu, X. Li, R. Li, M. Cai, T.-K. Sham, X. Sun, *J. Mater. Chem. A* **2014**, *2*, 2306 – 2312.
[32] X. Meng, Y. Zhong, Y. Sun, M. N. Banis, R. Li, X. Sun, *Carbon* **2011**, *49*, 1133 – 1144.
[33] X. Li, J. Liu, X. Meng, Y. Tang, M. N. Banis, J. Yang, Y. Hu, R. Li, M. Cai, X. Sun, *J. Power Sources* **2014**, *247*, 57 – 69.
[34] X. Li, J. Liu, M. N. Banis, A. Lushington, R. Li, M. Cai, X. Sun, *Energy Environ. Sci.* **2014**, *7*, 768 – 778.
[35] S. Stambula, N. Gauquelin, M. Bugnet, S. Gorantla, S. Turner, S. Sun, J. Liu, G. Zhang, X. Sun, G. A. Botton, *J. Phys. Chem. C* **2014**, *118*, 3890 – 3900.
[36] J. Liu, M. N. Banis, X. Li, A. Lushington, M. Cai, R. Li, T.-K. Sham, X. Sun, *J. Phys. Chem. C* **2013**, *117*, 20260 – 20267.
[37] X. Li, J. Liu, B. Wang, M. N. Banis, B. Xiao, R. Li, T.-K. Sham, X. Sun, *RSC Adv.* **2014**, *4*, 27126 – 27129.
[38] X. Li, X. Meng, J. Liu, D. Geng, Y. Zhang, M. N. Banis, Y. Li, J. Yang, R. Li, X. Sun, M. Cai, M. W. Verbrugge, *Adv. Funct. Mater.* **2012**, *22*, 1647 – 1654.
[39] X. Han, Y. Liu, Z. Jia, Y.-C. Chen, J. Wan, N. Weadock, K. J. Gaskell, T. Li, L. Hu, *Nano Lett.* **2014**, *14*, 139 – 147.
[40] Y. S. Jung, A. S. Cavanagh, L. A. Riley, S.-H. Kang, A. C. Dillon, M. D. Groner, S. M. George, S.-H. Lee, *Adv. Mater.* **2010**, *22*, 2172 – 2176.
[41] D. Buchholz, L. G. Chagas, M. Winter, S. Passerini, *Electrochim. Acta* **2013**, *110*, 208 – 213.
[42] X. Ma, H. Chen, G. Ceder, *J. Electrochem. Soc.* **2011**, *158*, A1307 – A1312.
[43] H.-M. Cheng, F.-M. Wang, J. P. Chu, R. Santhanam, J. Rick, S.-C. Lo, *J. Phys. Chem. C* **2012**, *116*, 7629 – 7637.
[44] G. Li, Z. Yang, W. Yang, *J. Power Sources* **2008**, *183*, 741 – 748.
[45] S. Amaresh, K. Karthikeyan, K. J. Kim, M. C. Kim, K. Y. Chung, B. W. Cho, Y. S. Lee, *J. Power Sources* **2013**, *244*, 395 – 402.
[46] K. Park, D. Han, H. Kim, W.-s. Chang, B. Choi, B. Anass, S. Lee, *RSC Adv.* **2014**, *4*, 22798 – 22802.
[47] H. Song, N. Li, H. Cui, X. Wen, X. Wei, C. Wang, *CrystEngComm* **2013**, *15*, 8537 – 8543.
[48] X. Xiao, P. Lu, D. Ahn, *Adv. Mater.* **2011**, *23*, 3911 – 3915.
[49] S. Malmgren, K. Ciosek, M. Hahlin, T. Gustafsson, M. Gorgoi, H. Rensmo, K. Edström, *Electrochim. Acta* **2013**, *97*, 23 – 32.

Received: January 29, 2015
Revised: March 15, 2015
Published online on June 26, 2015